Electric-Field-Triggered Ion Trapping for Non-Volatile Doping of Graphene Transistors

Dnyanesh Deepak Sarawate
University of Pittsburgh
Priscilla Prem
University of Pittsburgh
Eric Beckmen
University of Pittsburgh
Ke Xu
Rochester Institute of Technology
Susan Fullerton-Shirey
fullerton@pitt.edu

University of Pittsburgh

Article

Keywords:

Posted Date: April 23rd, 2026

DOI: https://doi.org/10.21203/rs.3.rs-9248175/v1

Additional Declarations: No competing interests reported.

Electric-Field-Triggered Ion Trapping for Non-Volatile Doping of Graphene Transistors

Dnyanesh D. Sarawate,[†] Priscilla M. Prem,[†] Eric J. Beckman,[†] Ke Xu,[*,‡,¶] and Susan K. Fullerton-Shirey[*,†,§]

[†]*Department of Chemical and Petroleum Engineering, University of Pittsburgh, Pittsburgh, PA*

[‡]*School of Physics and Astronomy, Rochester Institute of Technology, Rochester, NY*

[¶]*Microsystems Engineering, Rochester Institute of Technology, Rochester, NY*

[§]*Department of Electrical and Computer Engineering, University of Pittsburgh, Pittsburgh, PA*

E-mail: ke.xu@rit.edu; fullerton@pitt.edu

Abstract

Polymorphic electronics, in which circuits dynamically alter their function, are a promising approach for secure, fault-tolerant, and adaptive computing systems. A major challenge is developing reconfigurable components that can maintain their new state without requiring constant power. Here, we demonstrate non-volatile doping of graphene field-effect transistors by trapping ions within the electric double layer (EDL) at room temperature using an electric-field-sensitive solid polymer electrolyte. The electrolyte is designed to both facilitate ion motion and undergo the Menshutkin reaction, triggered by the large electric fields generated by the EDL itself. The reaction crosslinks the polyethylene oxide (PEO)-based copolymer and traps ions at the interface between the electrolyte and the channel, giving rise to persistent channel doping that remains after grounding the gate terminal. Applying a positive programming

voltage induces stable, n-type doping; however, negative programming voltages induce only weak, counter-doping, underscoring the asymmetry between positive and negative biasing. Low-temperature, dual-gated measurements confirm that ion trapping leads to non-volatility by distinguishing mobile, bulk ions from those trapped at the interface. Programming at ±5 V induces a change in electron sheet carrier density on the order of $\sim 10^{12}\,\mathrm{cm}^{-2}$, with only weak dependence on the ion concentration. The programmed states show an average retention of the induced sheet-carrier density of 80% over seven weeks at ambient conditions; the induced charge remains stable over the first week, but starts to fluctuate by ±20% in the last four weeks. This work demonstrates a new solid electrolyte with field-sensitive functionality, and provides a device-level path for the development of electrically reconfigurable logic elements relevant to polymorphic electronics and next-generation computing.

1. Introduction

The doping profile of a silicon transistor is established during fabrication, meaning that each device is set to favor transport of a majority charge carrier, and this doping defines its subsequent function in a logic gate. In contrast, a polymorphic transistor would enable individual devices to be programmed and even reprogrammed on demand using an external stimuli, like an electric field.[1] In this case, a transistor could be programmed n- or p-type, or switched from n- to p-type and visa versa using a gate. Such reconfigurability would introduce a new level of adaptability in circuit design, allowing for dynamic reassignment of functionality without the need to replace hardware. This could be useful for hardware security, fault-tolerant architectures, and adaptive computing systems where circuit functionality needs to evolve post-fabrication.[2–6] A key challenge, however, is realizing such reconfigurability without continuous power consumption or reliance on external stimuli.

While a silicon transistor itself is not polymophic, multiple silicon transistors can be combined to create a polymorphic circuit. For example, between 6 to 16 transistors have

been combined to demonstrate circuits that switch between NAND/NOR and AND/OR.[7–9] Beyond silicon, polymorphic circuits have been demonstrated in emerging materials such as WSe_2,[10,11] silicon nanowires,[12,13] and black phosphorous using only four transistors.[14,15] Fewer transistors are required because - unlike silicon - these semiconductors are ambipolar and can therefore be switched between p- and n-type on demand. This is accomplished by adding a programming gate (in addition to the control gate that turns the device off and on), which controls n- or p-type carrier injection by tuning the Schottky barrier height. This device is sometimes referred to as a Schottky barrier FET (SB-FET). While promising, the programming gate of an SB-FET needs to be applied continuously, making dynamic power consumption and delay time a challenge.[15]

A more desirable design would be a transistor for which channel doping can be set to p- or n-type after fabrication using a programming gate that does not need to be continuously applied during operation. That is, a transistor that can undergo programmable and non-volatile doping. Moreover, programming would be accomplished by addressing the transistor electrically, and not, for example, using thermal energy or photons which significantly increase overhead.[12]

One type of transistor in which doping can be dynamically modulated is an electric double layer transistor (EDLT), where mobile ions in an electrolyte form an interfacial electric double layer that electrostatically dopes the channel. Such gating is widely used to explore transport in semiconductors, because of large capacitance densities $\sim$ 1–15 $\mu F cm^{-2}$[16–18] that can induce large sheet carrier densities in range of $\sim 10^{13} - 10^{14} cm^{-2}$.[19–21] However, the doping is volatile, meaning that once the gate bias is removed, the mobile ions relax back to their equilibrium positions within the electrolyte, and the channel loses its induced carriers. This volatility prevents long-term retention of the programmed state, and limits usefulness in a potential application such as polymorphic transistors.

Efforts have been made to impart some degree of non-volaitility in EDLTs. The most common approach is to create an EDL with the programming gate and then decrease the

temperature of the device below the glass transition temperature (T_g) of the polymer. This approach exploits the coupling between ion mobility and the segmental mobility of the polymer backbone.[22–24] EDLs formed at $T > T_g$ are effectively locked into place at $T < T_g$, meaning that the doping will persist even after the gate voltage is removed. However, the T_g is typically well below room temperature ($< -40°C$), meaning that low temperatures are required to achieve such ion trapping. Our group has demonstrated room-temperature EDL locking using a polymer with a $T_g >$ room temperature; however, programming the device requires heating to 100 °C.[25] Another method to decrease segmental mobility and trap EDLs is by covalently crosslinking the polymer backbone.[26] Room-temperature crosslinking, both thermal- and photo-initiated, has been used to trap EDLs by us[27,28] and others.[29] However, this approach requires heat or light to be applied by either an external or on-board source, reintroducing additional energy overhead that undermines the goal of electrically programmable, low-power reconfigurability.

In this work, we introduce a new type of solid-state electrolyte called an electric-field sensitive polymer electrolyte. Similar to conventional electrolytes, applying a gate voltage induces EDL formation that heavily dopes the channel; however, the field-sensitive electrolyte also undergoes a chemical reaction to trap the ions - and therefore the induced charge in the channel - in response to the large electric field (i.e., V/nm)[19] generated by the EDL. In other words, the EDL serves a dual role needed for a polymorphic transistor: to dope the channel on demand, and to generate the electric field that drives the chemistry to trap ions and impart non-volatile doping.

Electric-field-driven chemical reactions have been investigated for decades.[30,31] Similar to catalysts, electric fields are understood to lower energy barriers to reactions, in this case, by aligning molecular dipoles to facilitate favorable reaction pathways.[32] The strength of the applied field required to initiate such reactions depends on the nature of the chemical bonds involved, with stronger bonds requiring higher fields.[33,34] Conveniently, the magnitude of the electric fields reported to promote such reactions (1 to 10 mV/nm)[35] are comparable to the

interfacial electric fields generated by a fully formed EDL. Thus, the EDL-generated electric field can be leveraged to drive a reaction at the interface between the electrolyte and the channel. This enables both channel doping and ion trapping using only the device-operating electric field, without relying on continuous biasing or external thermal or optical stimuli.

In this work, we custom-synthesize a co-polymer that both conducts ions and undergoes polymer crosslinking via the Menshukin reaction. This reaction, which can also be driven by thermal energy, produces covalent crosslinks using electric fields.[33,36] When thermally activated, we show that the reaction increases the T_g of the co-polymer electrolyte by more than 20 °C, resulting in a nearly one order of magnitude decrease in the room-temperature ionic conductivity. When applied to graphene FETs, the electric fields generated by EDLs simultaneously dopes the FETs, and traps the ions with density to $\sim 10^{12}\, cm^{-2}$. The doping persists for days after the gate bias is removed, with 80% retained for several weeks, providing proof-of-concept for electrically triggered, on-demand programming and non-volatility in a single transistor.

2 Results and discussion

Each component of the co-polymer, 2-(diethyl amino) ethyl methacrylate-co-poly(ethylene glycol) methyl ether methacrylate, (poly(DEAEMA-co-PEGMA)), serves a function in the ion-trapping strategy. Because ion mobility is required for EDL formation, PEGMA includes ether oxygen atoms to coordinate with Li^+ and facilitate ion motion via polymer mobility.[32,33,37,38] The second part, DEAEMA, includes tertiary amines that combine with 1,6-dibromohexane (DBH) crosslinker via the Menshutkin reaction with DEAEMA:DBH molar ratio of 2:1. This crosslinking reaction covalently crosslinks the polymer and decreases ion mobility. The reaction scheme is depicted in Figure 1(a) in which two bromine anions are liberated, and the tertiary amine becomes a quaternary ammonium cation. The co-polymer is synthesized by free radical polymerization, and the resulting NMR spectra are provided in

Figure 1(b), confirming the structure and showing the side chain ratio of PEGMA:DEAEMA = 1:0.85.

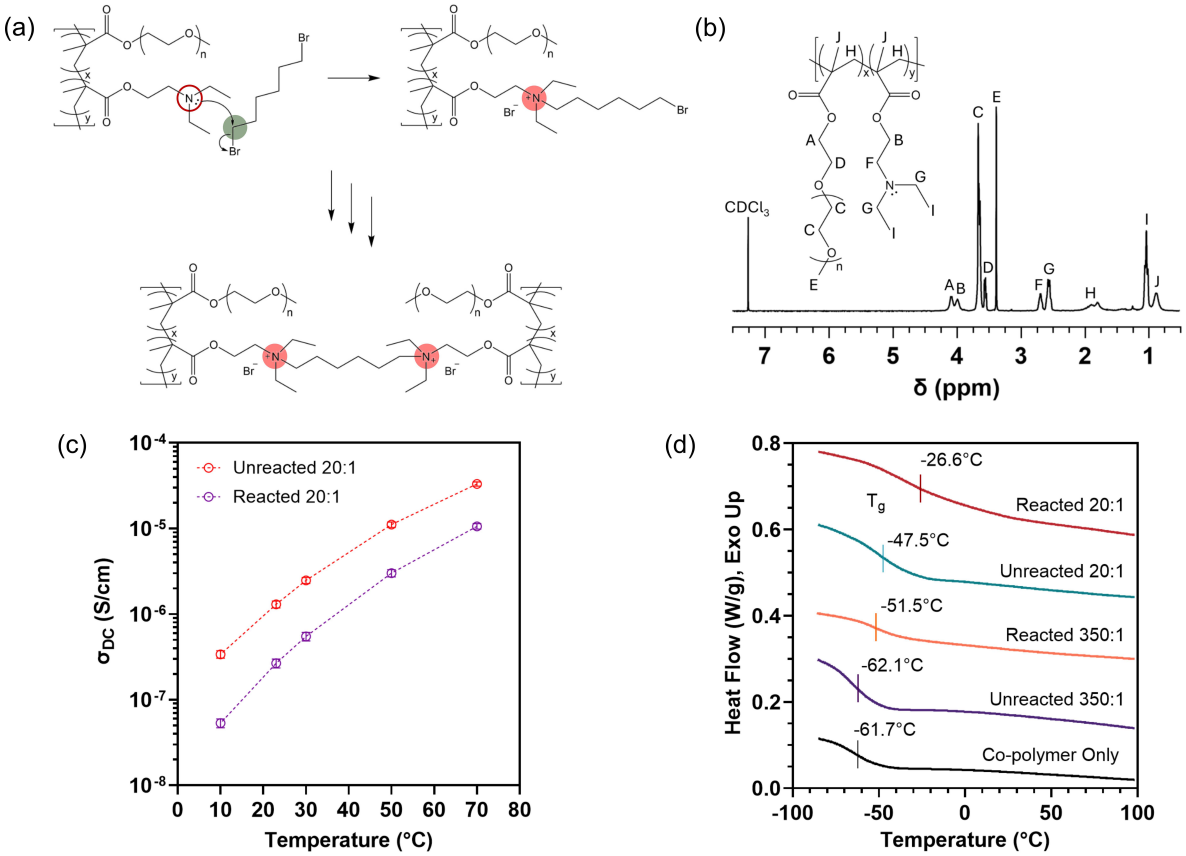

Figure 1: **Reaction schematic of poly(DEAEMA-co-PEGMA), ionic and thermal characterization of the electrolyte. (a)** Schematic of the Menshutkin crosslinking reaction between poly(DEAEMA-co-PEGMA) and DBH crosslinker. The tertiary amine (red, unfilled) of the co-polymer liberates a Br^- ion by reacting with the carbon atom (green) on the crosslinker, forming a quaternary ammonium cation (redfilled). **(b)** H^1 NMR spectra where each peak corresponds to a bonding environment of poly(DEAEMA-co-PEGMA). **(c)** Ionic conductivity of reacted and unreacted co-polymer with ether oxygen to Li^+ ratio of 20:1. **(d)** Differential scanning calorimetry measurements of the co-polymer without salt and reacted and unreacted electrolytes with salt concentrations of 20:1 and 350:1. T_g midpoint are indicated by vertical lines and the data are shifted along the y-axis for clarity.

The impact of crosslinking on ion mobility is measured in a metal-insulator-metal capacitor geometry using broadband dielectric spectroscopy (BDS). $LiClO_4$ is added to the co-polymer in an ether oxygen to Li^+ (EO:Li^+) ratio of 20:1, and the temperature-dependent DC conductivity (σ_{DC}) is measured before and after thermal crosslinking, Figure 1(c). σ_{DC}

is extracted from the frequency independent region of the conductivity spectra, calculated as:

$$\sigma(f) = \frac{\cos\theta(f)}{|Z|(f)}\frac{L}{A} \tag{1}$$

where $|Z|$ is the magnitude of the impedance, θ is the phase angle, f is frequency, L is the sample thickness, and A is the area. Frequency-dependent impedance and phase angle data, along with the calculated conductivity, are provided in Figure S1. The DC conductivity shows an Arrhenius temperature dependence, which is expected at measurement temperatures greater than T_g, which is -47 °C for an EO:Li^+ of 20:1 (Figure 1(d)). A 24 hour isothermal hold at 70 °C crosslinks the polymer, increasing T_g by 20° (Figure 1(d)). The increase in T_g reduces the polymer mobility at a fixed measurement temperature, resulting in a corresponding decrease in the ionic conductivity, shown in Figure 1(c).

The frequency range of the BDS measurements captures the resistive response of the electrolyte from which the ionic conductivity can be extracted, and does not explore the low-frequency capacitive contribution were EDL formation occurs. To confirm EDL dynamics, time-dependent current-voltage measurements are made using a lateral capacitor geometry on Si. Au contacts were deposited on SiO_2/Si, and a charging current was monitored in response to an applied voltage (Figure S2). A time constant of 3 seconds is extracted from the fit to a stretched exponential, which is of similar magnitude to that of the well-studied polymer electrolyte, PEO:$LiClO_4$ ($\sim$ 11 s, Figure S2(d)). These results imply that similar EDL gating dynamics should be observed between PEO and poly(DEAEMA-co-PEGMA).

The mechanisms of EDL gating and field-induced ion trapping are depicted schematically in Figure 2(a). When a positive gate voltage is applied, cations accumulate at the semiconductor surface and induce n-type doping in the channel (Figure 2(a)(ii)). As described in the introduction, the large electric fields ($\sim$V/nm) generated by the EDL is expected to trigger the Menshutkin reaction and immobilize ions in the EDL. This mechanism is depicted in Figure 2(a)(ii) where the programming gate (V_{PG}) is set to +5 V, a programming voltage se-

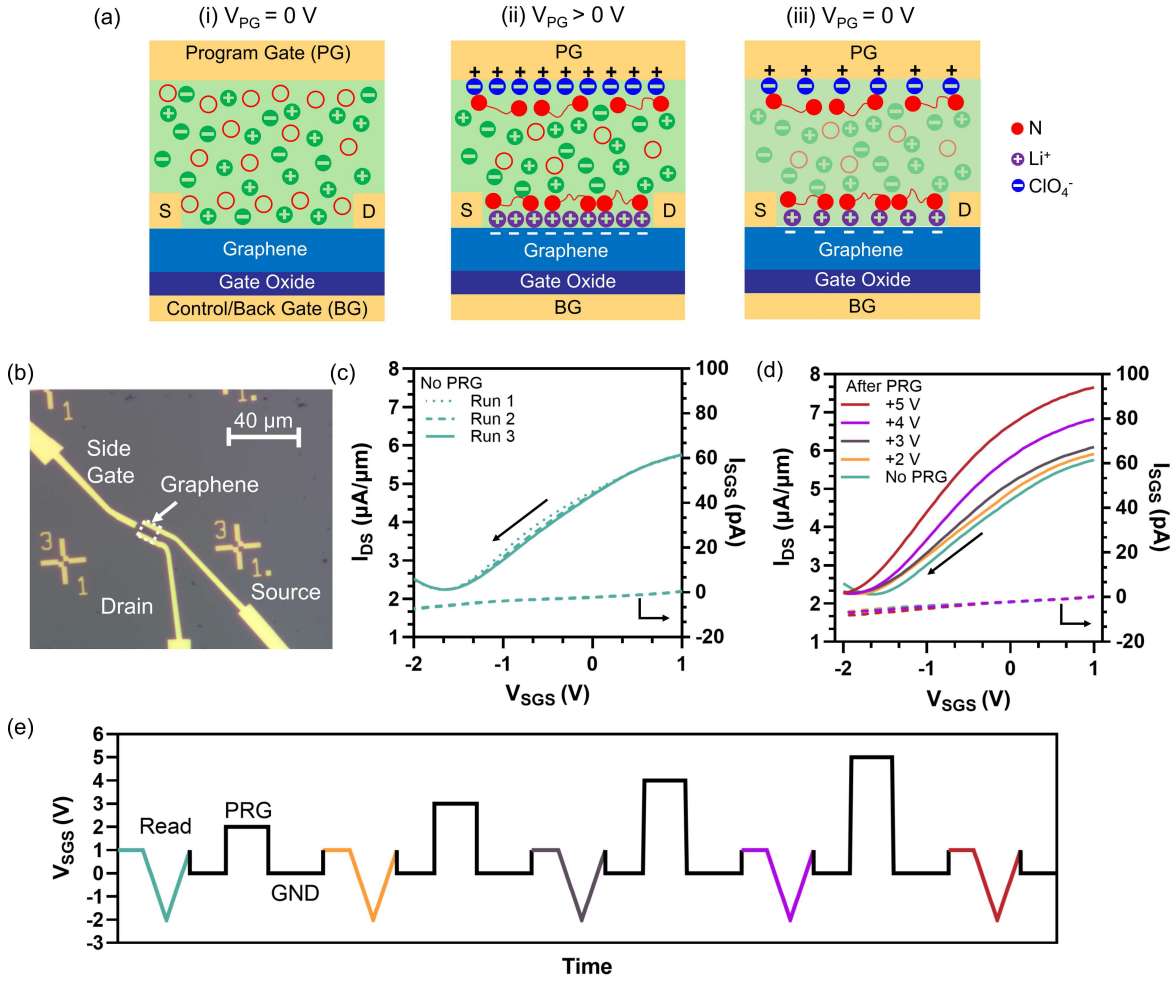

Figure 2: **Schematic and preliminary evidence of ion-trapping in the EDL (a)** Schematic of the proposed mechanism using poly(DEAEMA-co-PEGMA), $LiClO_4$ and a crosslinker on a transistor: **(i)** no gate bias applied, **(ii)** V_{PG} >0 V forming a cationic double layer that dopes the device n-type while also driving the crosslinking reaction, shown by red unfilled circles (tertiary amine) to red filled circles (quaternary ammonium cation) to trap the Li^+, **(iii)** gate terminal is grounded, V_{PG} =0 V, and n-type doping persists. **(b)** Optical image of a fabricated transistor prior to electrolyte deposition. Single-sweep, side-gated transfer characteristics of device D1 **(c)** before programming (three consecutive measurements) and **(d)** with no programming, and after programming with V_{PG} = +2, 3, 4, and 5 V bias using the programming sequence shown in **(e)**, with V_{DS} = 20 mV, T = 310K, and Sweep rate = 1 mV/s, EO:Li^+ = 350:1

lected by side gating experiments described below. Crosslinking is shown as covalent bonding between N atoms (red) in accordance with the reaction scheme of Figure 1(a). Crosslinking is expected to trap some fraction of the cations at the EDL such that doping persists even after V_{PG} is set to ground (Figure 2(a)(iii)) yielding non-volatile doping. As shown above in

Figure 1, the reaction can also be thermally induced; however, it requires high temperatures (T > 353 K)[39] or long time (time > 7 days).[40] All transistor measurements are taken at T < 310 K, and therefore no contributions from thermal crosslinking are expected.

Graphene was chosen as the channel material for its ambipolar conduction. The n- or p- type EDL will shift the Dirac point, and whether or not the shift persists after the gate contact is grounded will indicate doping volatility. Devices were fabricated by electron beam lithography on exfoliated flakes of thickness 0.7 to 3 nm; Figure 2(b) shows an optical image of a fabricated graphene transistor. The range of channel lengths/widths for all devices is 3–5/1–5 μm. Surface characterization using Atomic Force Microscopy (AFM) for the same is shown in Figure S3.

To study electric-field-induced ion trapping, we use two programming schemes. In the first, the side-gate (SG) is used for both device programming (i.e., the programming gate in Figure 1(a)) and for room-temperature transfer measurements. This scheme is used to determine the gate voltage at which ion trapping occurs, which corresponds to the minimum voltage required to induce the Menshutkin reaction. In the second scheme, the SG is used exclusively as the programming gate, and the back-gate (BG) is used for low-temperature transfer measurements. The two-step procedure decouples the programming from the electrical readout of the channel conductance (i.e., Dirac point location), and performing the readout at T < T_g of the polymer electrolyte eliminates any contribution of bulk ion conductivity to the channel doping. That is, only the ions that have been trapped at the interface will contribute to the doping.

2.1 Side-gate programming and readout

Before determining the programming voltage, a side-gate voltage range must be identified that can readout the channel conductance without driving the reaction. To establish such a read window, we repeatedly sweep V_{SG} over consecutively larger voltage windows while monitoring the Dirac point location between cycles. As shown in Figure 2(c), V_{SG} ranging

from −2 to +1 V yield consistent single-sweep transfer characteristics over three consecutive runs with no measurable shift in the Dirac point. (Double sweep transfer measurements are shown in Figure S4(a)) Thus, -2 to +1V is identified as the non-reactive read window.

Next, the programming voltage is identified using a four-step sequence (read–program–ground–read), where the voltage is increased by 1 V increments from +2 to +5 V. The full voltage sequence is provided in Figure 2(e). The hypothesis is that programming at voltages outside the read window will trap ions, and that the resulting Dirac point shift will remain after the program bias is removed and the gate is grounded. Figure 2(d) shows transfer characteristics for device D1 before programming, and after each voltage is applied for 30 minutes. The transfer measurements show modest n-type shifting at +2 and +3 V, suggesting very little reaction has occurred; however, at +4 V, the ON/OFF ratio increases, and the subthreshold swing (SS) improves, indicating enhanced gate coupling even after grounding the gate. Finally, at +5 V programming, a larger n-type Dirac point shift persists after grounding the gate. The shift suggests that +5 V is sufficient to induce the reaction and trap the ions, and +5 V programming of a second device, D2, shows similar results (Figure S4). Therefore, ±5 V is chosen as the programming voltages for subsequent measurements.

Sequential programming using gate voltages of opposite polarity is measured on two additional devices, D3 and D4. D3 is programmed at +5 V followed by −5 V, and D4 at −5 V followed by +5 V. Transfer characteristics of both devices and their corresponding programming sequences are provided in Figure 3. Similar to devices D1 and D2, an n-type shift is observed after the program–ground cycle of D3 using a programming voltage of +5 V. Applying a negative gate bias partially reverses the n-type doping, but does not shift the Dirac point back to the pre-programmed location (Figure 3a). Such a shift suggests that counterdoping by the anions is competing with cations trapped in the EDL.

Interestingly, when negative programming is applied first to device D4, there is only a very small n-type shift in the Dirac point. This result has two implications. First, the quaternary ammonium cations generated during the reaction do not contribute significantly

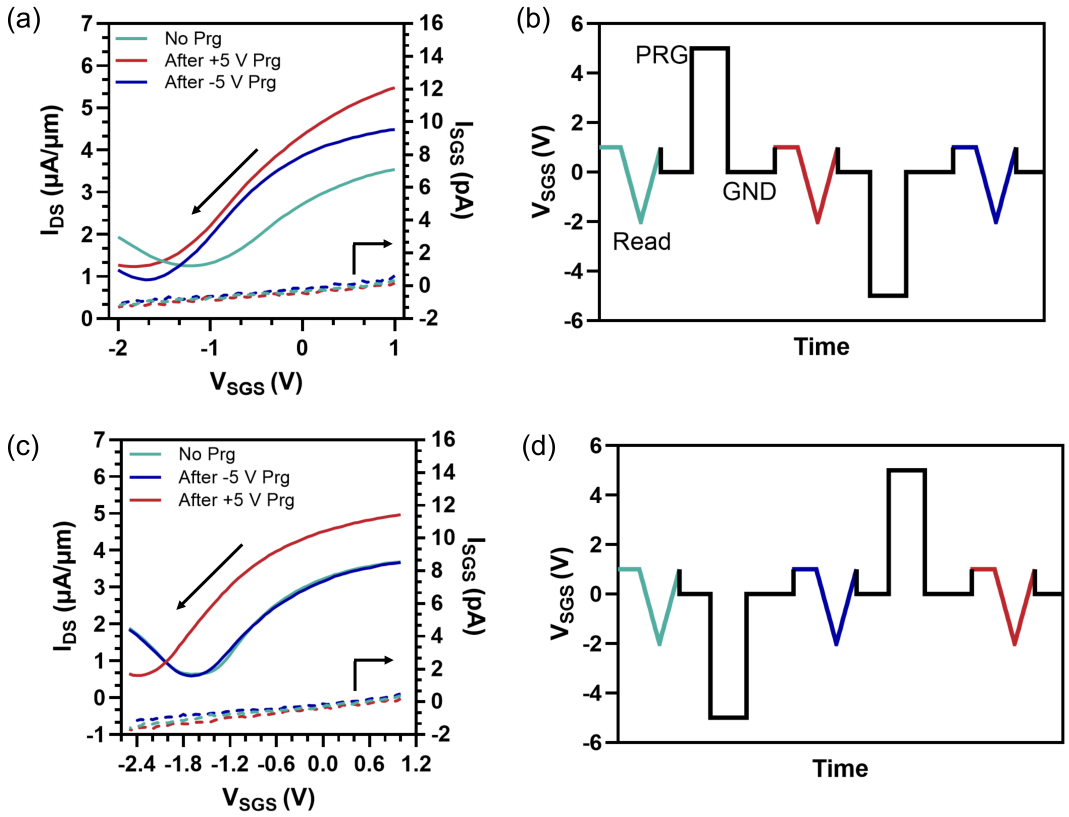

Figure 3: **Side-gated transfer characteristics and voltage profiles for programming and readout (a)** Single sweep side-gated transfer characteristics of device D3 unprogrammed (no prg), programmed with +5 V, and then programmed with −5 V as shown in the programming sequence **(b)**. **(c)** Single sweep side-gated transfer characteristics of device D4 when unprogrammed, programmed with −5 V, and then programmed with +5 V as shown in the programming sequence in **(d)**. EO:Li^+ = 350:1, V_{DS} = 10 mV, T = 296 K, and sweep rate = 1 mV/s

to the doping. Even though the tertiary amines outnumber the cations by 50 to 1 at an ether oxygen to Li^+ ratio of 350:1, they will contribute little to the doping because they are tethered to the polymer and therefore cannot drift in response to the applied field. Thus, only quaternary ammonium cations that happen to be close to the channel as the reaction proceeds are likely to contribute to n-type doping. The second implication is that the anions (whether they be ClO_4^- or liberated Br^-) are not trapped near the channel. In contrast, when a positive programming voltage is applied, the n-type shift returns and mirrors the characteristics of device D3. Such asymmetry – where cations are trapped at the channel,

but not anions – is unexpected. Although speculative, it could relate to the fact that anions, unlike cations, do not coordinate strongly with the polymer backbone as evidenced by larger diffusion coefficients for anions than cations in ether oxygen-based polymers.[41] Thus, anions are likely to be less impacted by decreased polymer mobility. Note that similar observations of the direction and magnitude of the Dirac point shifts are made on devices D1 and D2, programmed at 1 V increments (Figure S4 (b-d)). In total, consistent non-volatile doping behavior was observed across four transistors.

2.2 Side-gate programming and back-gate readout

In the measurements above, a single-gate programming scheme was used to immobilize a portion of the EDL using field-effect. However, single-gate operation requires limiting the gate-voltage sweep range during readout to avoid disturbing the programmed state. As a result, programming can shift the Dirac point outside the readout voltage window, thereby eliminating the possibility of extracting a reliable change in the sheet carrier density.

To overcome this limitation, we employed a dual-gate programming and readout sequence in which the back-gate is used exclusively for readout at low temperature. Programming continues to be carried out using the side-gate at room temperature (300 K), which is above the T_g of the polymer. After programming, all terminals are grounded at 300 K so that only doping induced by trapped ions remains. The devices are then cooled to 200 K to arrest ion mobility, and readout is performed using the back-gate. With this approach, the change in charge carrier density corresponds exclusively to the fixed charges trapped by programming. Furthermore, arresting the bulk ion mobility by decreasing the temperature prevents additional gate control that could be provided by ions in the bulk electrolyte.

Although 200 K is below the midpoint of the T_g (Figure 1(d)), the transition is broad, and the onset starts below the lowest temperature accessible by the differential scanning calorimetry (DSC) instrument used to measure T_g. Therefore, to pinpoint the onset of ion mobility, temperature-dependent transfer measurements are made from 153 to 323 K (Fig-

ure S5(a), (b)). The onset of gate control, and therefore ion-mobility, occurs near 233 K, confirming that ions will be immobile at 200 K. While modulating the temperature, we noticed a p-type Dirac point shift, even when floating the gate terminal (i.e., no programming). However, annealing the device at 300 K for 12 hours after cooling stabilizes this shift; the stabilization protocol is described in Part 3 of the Supplementary Information.

After confirming the bulk ion immobilization temperature, dual-gated measurements are made to quantify the Dirac point shift that arises from trapped ions. Two EO:Li^+ ratios, 350:1 and 20:1, were selected to evaluate the influence of ion concentration on the programming behavior. The forward (-40 V to 30 V) and reverse (30 V to -40 V) sweeps of the transfer measurements are presented in Figure 4 (b-e) for devices D5-D8. Devices D5 and D6 (Figures 4(b, c)) are gated with the 20:1 electrolyte concentration, while D7 and D8 (Figures 4(d, e)) are gated with 350:1. The programming of devices D5 and D7 follow the protocol in 4(a) using +5 V first followed by −5 V, and the polarity sequence is reversed for D6 and D8. Devices are first programmed at 300 K using the side-gate then all terminals are grounded. The devices are cooled to 200 K, and transfer measurements are recorded using the back-gate. A small hysteresis is observed only for device D6 and only after negative programming, which is not present prior to programming or following subsequent positive programming. All other devices measured at 200 K exhibit negligible hysteresis. The isolated nature of this behavior suggests device-specific contact non-idealities, which are known to introduce variability in graphene FET transfer characteristics.[42]

The Dirac point location (V_{DP}) was identified from the transfer characteristics (I_D vs. V_{BG}), defined as the gate voltage corresponding to the minimum drain current. For device D6, due to the hysteresis observed after −5 V programming, the Dirac point was determined by taking the average of the two Dirac point voltages obtained from the forward and reverse sweeps. The left and right shifts of the Dirac point in response to programming are summarized for each device in Figure 5(a). Note that the shift is always shown relative to the device's Dirac point location from the prior programming.

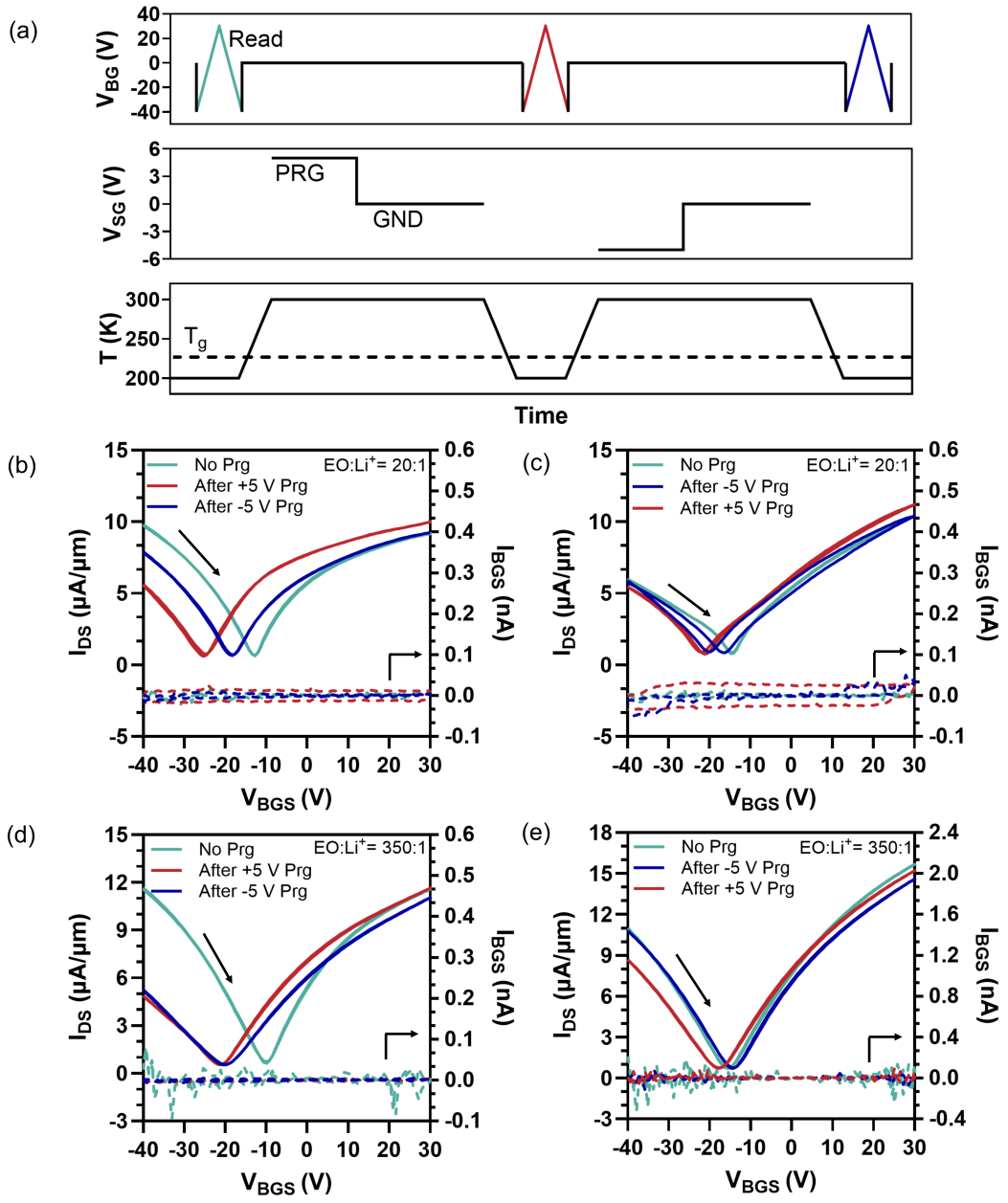

Figure 4: **Back-gated transfer characteristics measured at 200 K after programming at room temperature.** **(a)** Programming sequence for devices D5 and D7. Back-gated, double-sweep transfer characteristics of **(b)** device D5 with EO:Li^+ = 20:1 and **(d)** device D7 with EO:Li^+ = 350:1 when unprogrammed (no prg), programmed with +5 V, and then programmed with −5 V. Back-gated double-sweep transfer characteristics of **(c)** device D6 with EO:Li^+ = 20:1 and **(e)** device D8 with EO:Li^+ = 350:1 when unprogrammed, programmed with −5 V, and then programmed with +5 V. V_{DS} = 10 mV and sweep rate ≈ 3 - 7 V/s.

For device D5 in Figure 4(b), a shift in the Dirac point (ΔV_{DP}) of -12.6 V is measured after room temperature programming at $+5$ V followed by grounding, confirming persistent channel doping after removal of the programming bias. Subsequent programming with -5 V partially reverses this n-type doping with a $\Delta V_{DP} = +7$ V. The Dirac point does not return to its original position, indicating that a substantial fraction of the programmed doping remains even after intentional reverse programming. In other words, the doping induced by positive programming is only partially undone with negative programming. The loss of n-type doping after reverse programming could be explained by the previously trapped cations being driven away, counter-doping by anions giving a p-type shift, or some combination thereof.

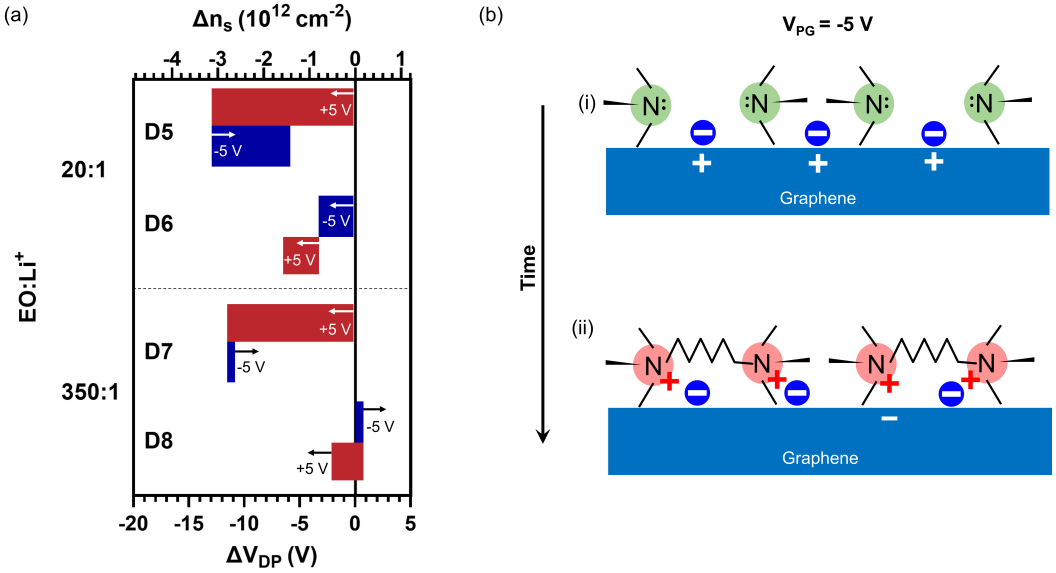

Figure 5: **Dirac point shift, charge density, and Proposed mechanism for reaction. (a)** Change in Dirac point (ΔV_{DP}) and corresponding change in electric-field triggered ion-trapped density (Δn_s) for the four devices (D5–D8) at varying ion concentrations after program-ground sequence. Both ΔV_{DP} and Δn_s are provided with respect to the unprogrammed measurement of each device. The programming steps are applied sequentially in the order shown from top to bottom for each device number. **(b)** Proposed ion distribution near the graphene surface (i) before the reaction and (ii) after reaction for -5 V programming.

To assess the role of programming sequence, a new device – device D6 – was programmed

using the same voltages but with polarity reversed (i.e., −5 V followed by +5 V). The results are shown in Figure 4(c). In response to −5 V programming, accounting for the hysteresis by taking the average of the two Dirac point voltages leads to a small ($\Delta V_{DP} = -3.15$ V) n-type shift, and an additional n-type shift ($\Delta V_{DP} = -4.9$ V) with subsequent +5 V programming. This behavior is counterintuitive because negative biasing would typically induce a p-type shift. Instead, the device exhibits an n-type response. Although speculative, it is possible that the quaternary ammonium cations are contributing more significantly to the doping at 20:1 compared to 350:1 because of the larger bulk ion concentration. Finite element modeling shows that the character of the EDL is relatively independent of bulk on concentration in the range of 10:1 and 50:1;[43] however, 350:1 is about 20 times more dilute and it is not unreasonable to expect that the field – and therefore the extent of reaction – will be smaller. Thus, at higher ion concentrations, the reaction causes the backbone of the polymer to compete more effectively with anions to dope the channel, as depicted schematically in Figure 5(b).

Furthermore, the total Dirac point shift following the subsequent +5 V programming step is more than 50% smaller than the shift obtained when positive programming is applied first (device D5, Figure 4(b)). The reduced net response suggests that when the device is programmed with negative bias first, anions are not well trapped at the surface, but the crosslinking prevents cations from making it to the surface during subsequent positive programming. The result is a weaker n-type shift than when positive programming is applied first. The microscopic mechanism underlying this sequence cannot be understood from transport measurements alone and would require further investigation via interfacial chemical characterization.

The same programming sequences were applied to devices D7 and D8, but with lower salt concentration (EO:Li^+ = 350:1). The transfer characteristics of device D7 in Figure 4(d) show that, just as for the 20:1 sample, the +5 V induces a pronounced n-type shift in the Dirac point ($\Delta V_{DP} = -11.2$ V), comparable to that observed in D5. This observation con-

firms that a similar extent of n-type doping persists even when the bulk ion concentration is 17.5 times lower. However, subsequent application of −5 V results in only a minor loss of the n-type doping ($\Delta V_{DP} = +0.7$ V). This contrasts the 20:1 concentration, where approximately 55% of the n-type shift was lost on negative programming, suggesting that the lower ion concentration is more stable against reversal, although it is not immediately clear why this would be the case.

Device D8 (−5 V followed by +5 V) shows a negligible response to the initial −5 V programming (Figure 4(e)), resulting in only a small positive shift in the Dirac point ($\Delta V_{DP} = +0.7$ V), indicative of weak p-type doping. Notably, this is the only instance of a p-type shift observed across all devices and programming sequences. This behavior contrasts with that of device D6, where an n-type shift was observed on the first negative programming. As hypothesized above, such an observation would be consistent with a reduced extent of reaction, and therefore fewer positively charged amines to counteract the p-type doping. Subsequent +5 V programming results in a comparatively small negative shift ($\Delta V_{DP} = -2.8$ V), similar to the observation in Figure 4(c).

To confirm that the Dirac point shifts arise from ion-trapping via field-induced crosslinking, control experiments are carried out with the identical polymer electrolyte but without the DBH crosslinker. No measurable shift in the Dirac point is observed with programming (Figure S6).

The change in carrier density is calculated based on the extracted Dirac point shifts using Equation 2

$$\Delta n_s = \frac{\Delta Q}{e} = \frac{C_{ox} \Delta V_{DP}}{e} \tag{2}$$

where $C_{ox}(38.7 nF/cm^2)$ is the capacitance of the 90 nm of SiO_2,[44] ΔV_{DP} is the difference between the Dirac point location after programming and the last reference point in the programming sequence, and e is the elementary charge. The calculated changes in the sheet carrier density for each device and programming polarity are provided in Figure 5(a). These

values reflect the trapped interfacial ionic charge density responsible for the non-volatile electrostatic doping of the graphene channel.

At EO:Li^+ = 20:1, positive programming (+5 V) produces a strong and persistent n-type response, with retained sheet carrier densities reaching $\sim 3 \times 10^{12}\,\mathrm{cm}^{-2}$ after the gate terminal is set to ground. This confirms that a substantial fraction of the EDL charge can be trapped, leading to non-volatile doping. In contrast, applying −5 V first results in significantly smaller induced carrier densities, and subsequent +5 V programming does not fully recover the maximum attainable density observed under positive-first operation. This pronounced history dependence indicates that the initial bias establishes an interfacial ionic configuration that constrains subsequent charge trapping as discussed previously and represented in Figure 5(b).

Importantly, the extracted densities represent only the *trapped* charge remaining after removal of the programming voltage. Under conventional EDL gating with continuous bias, carrier densities on the order of 10^{13}–$10^{14}\,\mathrm{cm}^{-2}$ are routinely achieved. The observation of up to $\sim 3 \times 10^{12}\,\mathrm{cm}^{-2}$ in the absence of an applied field therefore indicates that a significant fraction of the EDL charge can be trapped using the electric-field-driven reaction mechanism.

To quantify the extent of non-volatility, we evaluate the temporal stability of the Dirac point. The location of the Dirac point is monitored as a function of time for device D7 in Figure 6. After completing the programming sequence shown in Figure 4(a), the device was stored at room temperature and periodically cooled to 200 K to perform low-temperature transfer measurements. Because the room temperature storage time was significantly longer than the measurement time at 200 K, these results reflect the room temperature state retention of the device. Short-term retention was evaluated using 4-hour storage intervals during the first three days, while longer storage durations were used subsequently to assess extended-time stability.

The uncertainty in V_{DP} was estimated by identifying the gate-voltage range over which the drain current remained within 10% of its minimum value; this range is reported as

the error bars in Figure 6. During the first three days, the device exhibits a loss of the n-type doping corresponding to $2.92 \times 10^{11}\,\mathrm{cm}^{-2}$. Over the subsequent seven weeks, the average retention remains approximately constant, maintaining about 80% of the initially programmed state. During the final four weeks, the retained state exhibits fluctuations of approximately ±20% around this average value.

Although complete immobilization of the EDL, which would lead to indefinite retention without measurable charge decay is not observed, the retention measurements clearly demonstrate ion trapping on experimentally relevant timescales. An average of 80% of the initially programmed charge density remains after seven weeks at room temperature. This behavior is different from what is expected with permanent ion-locking mechanisms that rely on thermally or photo-initiated crosslinking, where complete non-volatility may be expected. It is also different from PEO-based electrolytes, where the EDL dissipates over tens of milliseconds[45] to seconds.[46] Instead, the applied electric field drives the formation of metastable, partially trapped, ionic configurations at the electrolyte/graphene interface, leading to a timescale of weeks to relax to 80% of its initial value, an increase in the relaxation time of $> 10^8$.

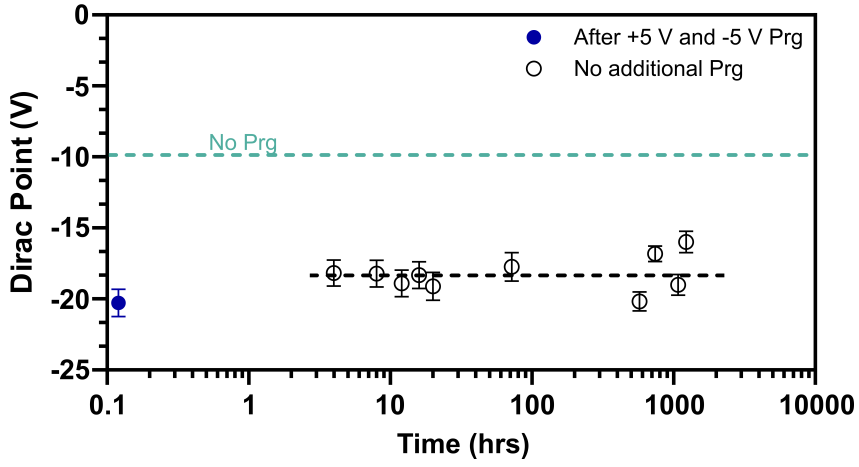

Figure 6: **Room-temperature doping retention for device D7 after programming.** The Dirac point location is extracted from transfer measurements taken at 200 K with $V_{DS} = 10\ mV$ and Sweep rate ≈ 3 - 7 V/s. Between measurements, the device is stored at room temperature.

3. Conclusions

In this work, we demonstrate electrically triggered, non-volatile electrostatic doping in graphene field-effect transistors using a custom solid polymer electrolyte. Rather than relying only on reversible electrostatic gating, the approach leverages an electric-field-sensitive Menshutkin reaction in a PEO-based copolymer, poly(DEAEMA-co-PEGMA), to induce polymer crosslinking at the electrolyte-graphene interface. This interfacial modification allows charges in the EDL to become effectively trapped, leading to a persistent change in the carrier density of the graphene channel even after removal of the programming bias.

A key observation is the strong asymmetry between the sequence of positive and negative programming. When the positive gate bias (+5 V) is applied first, it results in stable and long-lived n-type doping for EO:Li^+ ratios of 20:1 and 350:1. In contrast, applying a negative bias (−5 V) first leads only to weak p-type doping for EO:Li^+ = 350:1, and weak n-type doping for EO:Li^+1 = 20:1. This limited doping can possibly be attributed the reaction-generated quaternary ammonium cation, which may compete with anions. Furthermore, even after the subsequent application of a positive bias (+5 V), the channel is not doped n-type for either concentration. This result suggests that the non-volatile doping behavior is strongly governed by the sequence of polarity bias applied, which triggers the reaction and traps ions at the graphene–electrolyte interface. Low-temperature and dual-gate measurements further support this picture by separating the contribution of trapped interfacial ions from that of mobile ions in the bulk electrolyte, confirming that the retained doping is not due to slow ion dynamics. For both EO:Li^+ ratios, positive programming (+5 V) induced a change in sheet carrier densities in the order of 10^{12} cm^{-2}, whereas negative programming (−5 V) induced change in sheet carrier densities in order of 10^{11} cm^{-2}, further confirming the weak doping by negative programming bias. The underlying mechanism for this asymmetry is unclear.

The demonstrated carrier densities and retention times indicate that this chemically assisted gating approach can reach a change in carrier densities sufficient to produce stable and polarity-selective shifts in ambipolar channels. Although the electrolyte is demonstrated

on graphene transistors, there is no evidence to suggest that the mechanism is unique to graphene. Even though the average retention of induced doping decreases to $\approx$ 80% of initially induced charges on a time scale of seven weeks, the results indicate non-volatility tuning can be achieved through the use of this solid polymer electrolyte.

More broadly, this study suggests that electric-field-induced interfacial reactions can be harnessed to enable reconfigurable electronic elements. With further development, such devices could be used as basic building blocks for polymorphic electronics, where logic functionality can be altered and retained without continuous power, opening up possibilities for adaptive and fault-tolerant computing architectures.

4. Materials and Methods

4.1 Fabrication of Graphene Field Effect Transistors

Graphene transistors were fabricated on 90 nm silicon oxide on p-doped Si (Graphene Supermarket). Alignment markers were defined on the Si substrate using a maskless aligner (Heidelberg MLA100 Direct Write Lithographer). Graphene was then exfoliated using the Scotch tape method, and flakes of uniform thickness ($\sim$0.7 - 2 nm) were identified using optical microscopy and atomic force microscopy (AFM, Bruker Dimension Icon). Source, drain, and side-gates were patterned using Electron Beam Lithography (EBL, Raith e-LiNE or Raith EBPG5150 100kV). First, PMMA resist was spin-coated (4000 rpm for 60 sec) followed by baking at 175 °C for 7 minutes. Written samples were developed first in a solution of methyl isobutyl ketone (MIBK) and isopropyl alcohol (IPA) in the volume ratio of 1:3 for 60 seconds, and then in pure IPA for 60 seconds. Next, metal contacts were evaporated (Plassys Electron Beam Evaporator, MEB550S) as 5/145 Ti/Au. The sample was soaked overnight in acetone for the lift-off. Following FET fabrication, AFM scan was performed in tapping mode to characterize the surface topography of the graphene channel. In cases where significant resist residue remained (Rq $>$ 1 nm) from the electron beam lithography

(EBL) process, contact mode AFM was subsequently employed for mechanical cleaning of the channel surface, which is known to increase the on current by 247%.[47] AFM images are shown in Figures S3 (a) and (b) with height profile in (c) and transfer characteristics in (d).

4.2 Polymer synthesis and electrolyte preparation

The co-polymer, poly(DEAEMA-co-PEGMA), consists of 2-(diethyl amino) ethyl methacrylate (DEAEMA, Sigma Aldrich) and poly(ethylene glycol) methyl ether methacrylate (PEGMA, M_n = 300 g/mol, Sigma Aldrich) monomers. The poly(DEAEMA-co-PEGMA) co-polymer was synthesized using a 1:1 molar ratio of DEAEMA to PEGMA monomers using a previously reported synthesis.[48,49] DEAEMA (2.78 g) and PEGMA (4.34 g) monomers were filtered through activated aluminum oxide (neutral Brockmann I, Sigma Aldrich) to remove inhibitors, dissolved in 20 mL toluene ($\geq$ 99.5 %, Sigma Aldrich), and deoxygenated with Ar gas for 30 min. Recrystalized azobisisobutyronitrile (AIBN, Sigma Aldrich) initiator was added in a 200:1 molar ratio of monomers, and the polymerization occurred under an Ar environment at 70 °C for 18 hours with constant stirring (400 rpm). The reaction was quenched in an ice bath, and the copolymer was precipitated in five-fold excess of cold n-hexane (Sigma Aldrich), dried in a fume hood for 3 days, and vacuum-dried at 26 inHg vacuum (Fisher-Brand Model 281A Vacuum Oven) at room temperature for 2 days before storing in an Ar-filled glovebox. The polymer electrolyte was prepared by dissolving 1 wt.% of the solid components–poly(DEAEMA-co-PEGMA), 1,6-dibromohexane (DBH, 96%, Sigma Aldrich), and salt ($LiClO_4$)–in anhydrous acetonitrile (99.8%, Fisher Scientific) with a salt concentration of 350:1 or 20:1 in an Ar-filled glovebox. DBH was added to the electrolyte in a ratio of DEAEMA:DBH = 2:1. Films of $\approx 1\ \mu m$ were deposited by drop-casting 25 μL of the solution on Graphene FETs and annealing at 50 ° C for 5 min.

4.3 H^1 NMR

H^1 NMR samples were prepared by dissolving 0.3 g of p(DEAEMA-co-PEGMA) in 0.75 mL of deuterated chloroform ($CDCl_3$) containing a 0.03% (v/v) internal tetramethylsilane (TMS) reference (Sigma Aldrich). The structure of the copolymer was confirmed by H^1

NMR (Bruker AVANCE III). The instrument was operated with a 10-second delay to allow sufficient time for the molecules to re-randomize between scans.

4.4 Differential Scanning Calorimetry

Samples for DSC were prepared by dissolving 5 wt.% of the solid components in anhydrous acetonitrile. The resulting solutions were transferred to Teflon vials and left uncovered in a fume hood for three days to evaporate the solvent. Residual solvent was subsequently removed by vacuum drying at 26 inHg vacuum for 48 hours at ambient temperature. 10–20 mg of the dried electrolyte were placed into aluminum DSC pans (PerkinElmer) and hermetically sealed under an Ar atmosphere in a glovebox prior to analysis.

For samples containing DBH, thermal crosslinking reactions were conducted by heating the electrolyte in the pans at 70 °C for seven days in an oven. This extended reaction time was selected based on prior literature demonstrating that quaternization of DEAEMA monomers with 1-bromohexane proceeds slowly under mild conditions, requiring approximately six days at 56 °C under reflux in acetonitrile.[40] Polymerized DEAEMA, however, was shown to crosslink with DBH at 80 °C for 12 hours, but this polymer did not include PEGMA.[39] Furthermore, polymerized 2-(dimethylamino)ethyl methacrylate (PDMAEMA), a structurally similar but less sterically hindered tertiary amine polymer, has been reported to undergo quaternization with 1-bromohexane over 30–48 hours at temperatures between 60–70 °C.[50,51] Given the increased steric hindrance of DEAEMA relative to DMAEMA and the additional constraints imposed by copolymerization with PEGMA, a reaction duration of seven days at 70 °C was employed to promote maximal crosslinking.

The DSC instrument (TA Instruments Discovery DSC250) was calibrated using indium (TA Instruments) and adamantane (≥99%, Sigma-Aldrich) standards to ensure accurate thermal measurements across the temperature range of interest. Samples were analyzed alongside an empty aluminum reference pan using an autosampler. Thermal characterization was performed using heat/cool/heat cycles spanning -90 to 100 °C, with an initial equilibration at 40 °C. Heating and cooling rates were set to 10 and 5 °C min^{-1}, respectively,

and an isothermal dwell of 10 min at 100 °C was applied following the first heating segment. T_g transitions were identified using TRIOS software (TA Instruments).

4.5 Electrical characterization

Samples were prepared for BDS measurements by dissolving 40 wt.% of solid components in anhydrous acetonitrile in an Ar-filled glove box. After mixing, the samples were removed from the glove box and 50 μL of the electrolyte solution was deposited in the center of a 1-inch-diameter brass electrode. The sample was left in a fume hood overnight to dry, then vacuum-dried at 26 inHg vacuum for 24 hrs to remove excess solvent. A Teflon spacer (1-inch O.D.; 3/4-inch I.D.; 130 μm thickness) was used to confine the electrolyte and maintain thickness on the brass electrode. A second brass electrode was placed on top, and the film thickness was measured using a micrometer.

BDS measurements for the 20:1 electrolyte were performed using a Novacontrol Concept 80 impedance analyzer in the frequency range of 10^{-2} to 10^{7} Hz (0.1 V AC). Measurements were taken before and after crosslinking the samples by performing heat/cool/heat cycles from 10–70 °C at a ramp rate of 1 °C/min, with measurements collected in 20 °C intervals and at room temperature (23 °C). Reported BDS measurements refer to the second heating segment prior to crosslinking to remove thermal hysteresis, and during the first heating segment after crosslinking (after the samples were cooled). Crosslinking was performed in-situ by holding the temperature of the sample chamber at 70 °C for 24 hours, with measurements taken every 2 hours. A final thickness measurement was collected by subtraction after the BDS measurement.

The electrical characteristics of FETs were measured in a probe station (Lakeshore CRX-V) using semiconductor parameter analyzer (SPA, Keithley 4200A-SCS, and Keysight B1500A). The sample was transferred in a custom load-lock without exposing the sample to air. For back-gated transfer characteristics, the temperature was maintained at 200 K at a pressure of $\sim 5 \times 10^{-7}$ Torr. Side-gated transfer characteristics temperature was maintained at 300 K with same pressure.

Acknowledgement

The research was supported by the National Science Foundation (NSF, U.S.) under NSF-DMR-EPMD #2132006. Work performed in the University of Pittsburgh Nanofabrication and Characterization Core Facility (RRID: SCR_05124) and Dietrich School Materials Characterization Laboratory (RRID:SCR_025127), and services and instruments used in this project were graciously supported, in part, by the University of Pittsburgh. Thank you to Henry Sun from Prof. Jennifer Laaser's lab for assistance with BDS sample preparation and measurements.

Data Availability

All data supporting the findings of this study are available within the paper and its Supplementary Information.

Author Contributions

Conceptualization, S.K.F.-S., K.X., E.J.B.; device fabrication, D.D.S.; device characterization and electrical measurements, D.D.S.; polymer synthesis and characterization, P.M.P. The manuscript was written through the contributions of all authors. All authors have given approval to the final version of the manuscript.

Supporting Information Available

The Supplementary Information is available free of charge at:

Ion mobility and EDL dynamics measurements; AFM surface characterization of graphene transistors; additional electrical measurements of side-gate programming and readout; thermal response and stability of poly(pDEA-co-PEGMA); measurements of control devices.

References

(1) Mcdonald, J. T.; Kim, Y. C.; Grimaila, M. R. *Protecting Reprogrammable Hardware with Polymorphic Circuit Variation **.

(2) Hauck, S.; DeHon, A. *Reconfigurable computing : the theory and practice of FPGA-based computation /*; Morgan Kaufmann Publishers/Elsevier,: Amsterdam [The Netherlands] ;, 2008.

(3) Jian, G.; Mengfei, Y. Evolutionary fault tolerance method based on virtual reconfigurable circuit with neural network architecture. *IEEE Transactions on Evolutionary Computation* **2018**, *22*, 949–960.

(4) Gohari, S. An Overview of Online Fault Tolerance for FPGA Logic Blocks. *Arman Process Journal (APJ)* **2023**, *4*, 1–16.

(5) Kumar, R.; Divyanshu, D.; Khan, D.; Amara, S.; Massoud, Y. Polymorphic Hybrid CMOS-MTJ Logic Gates for Hardware Security Applications. *Electronics 2023, Vol. 12, Page 902* **2023**, *12*, 902.

(6) Bernard, C.; Bryant, W.; Becker, R.; Di, J. Design of Asynchronous Polymorphic Logic Gates for Hardware Security. *2021 IEEE High Performance Extreme Computing Conference, HPEC 2021* **2021**,

(7) Stoica, A.; Zebulum, R.; Keymeulen, D. Polymorphic Electronics. *Lecture Notes in Computer Science (including subseries Lecture Notes in Artificial Intelligence and Lecture Notes in Bioinformatics)* **2001**, *2210*, 291–302.

(8) Ruzicka, R.; Sekanina, L.; Prokop, R. Physical demonstration of polymorphic self-checking circuits. *Proceedings - 14th IEEE International On-Line Testing Symposium, IOLTS 2008* **2008**, 31–36.

(9) Stoica, A.; Zebulum, R. S.; Guo, X.; Keymeulen, D.; Ferguson, M. I.; Duong, V. Taking evolutionary circuit design from experimentation to implementation: some useful techniques and a silicon demonstration. *IEE Proc.-Comput. Digit. Tech.* **2004**, *151*, 295–300.

(10) Wu, P.; Reis, D.; Hu, X. S.; Appenzeller, J. Two-dimensional transistors with reconfigurable polarities for secure circuits. *Nature Electronics* **2021**, *4*, 45–53.

(11) Tang, C. S.; Yin, X.; Wee, A. T. Polymorphic two-dimensional transition metal dichalcogenides: Modern challenges and opportunities. *Two-Dimensional Transition-Metal Dichalcogenides: Phase Engineering and Applications in Electronics and Optoelectronics* **2023**, 295–324.

(12) Lee, S. J. et al. Programmable devices based on reversible solid-state doping of two-dimensional semiconductors with superionic silver iodide. *Nature Electronics* **2020**, *3*, 630–637.

(13) Ghosh, S.; Khan, M. B.; Prucnal, S.; Hübner, R.; Chava, P.; Mauersberger, T.; Mikolajick, T.; Erbe, A.; Georgiev, Y. M. High-Performance Silicon Nanowire Reconfigurable Field Effect Transistors Using Flash Lamp Annealing. *ACS Applied Electronic Materials* **2025**, *7*, 2284–2297.

(14) Malayee, F. M.; Bagheri, R.; Nazari, F.; Illas, F. Electrostatic Gating of Phosphorene Polymorphs. *Journal of Physical Chemistry C* **2024**, *128*, 2997–3010.

(15) Bi, Y.; Shamsi, K.; Yuan, J. S.; Gaillardon, P. E.; De Micheli, G.; Yin, X.; Hu, X. S.; Niemier, M.; Jin, Y. Emerging technology-based design of primitives for hardware security. *ACM Journal on Emerging Technologies in Computing Systems* **2016**, *13*.

(16) Efetov, D. K.; Kim, P. Controlling electron-phonon interactions in graphene at ultrahigh carrier densities. *Physical Review Letters* **2010**, *105*, 256805.

(17) Kim, S. H.; Hong, K.; Xie, W.; Lee, K. H.; Zhang, S.; Lodge, T. P.; Frisbie, C. D. Electrolyte-gated transistors for organic and printed electronics. 2013.

(18) Xia, Y.; Zhang, W.; Ha, M.; Cho, J. H.; Renn, M. J.; Kim, C. H.; Frisbie, C. D. Printed sub-2 V Gel-electrolyte-gated polymer transistors and circuits. *Advanced Functional Materials* **2010**, *20*, 587–594.

(19) Xu, K.; Fullerton-Shirey, S. K. Electric-double-layer-gated transistors based on two-dimensional crystals: Recent approaches and advances. 2020.

(20) Weintrub, B. I.; Hsieh, Y. L.; Kovalchuk, S.; Kirchhof, J. N.; Greben, K.; Bolotin, K. I. Generating intense electric fields in 2D materials by dual ionic gating. *Nature Communications* **2022**, *13*.

(21) Vasileska, D.; Schroder, D. K.; Ferry, D. K. Scaled silicon MOSFET's: Degradation of the total gate capacitance. *IEEE Transactions on Electron Devices* **1997**, *44*, 584–587.

(22) Bruce, P. G.; Vincent, C. A. Polymer electrolytes. *Journal of the Chemical Society, Faraday Transactions* **1993**, *89*, 3187–3203.

(23) Xu, H.; Fathipour, S.; Kinder, E. W.; Seabaugh, A. C.; Fullerton-Shirey, S. K. Reconfigurable ion gating of 2H-MoTe2 field-effect transistors using poly(ethylene oxide)-CsClO4 solid polymer electrolyte. *ACS Nano* **2015**, *9*, 4900–4910.

(24) Von Seggern, F.; Keskin, I.; Koos, E.; Kruk, R.; Hahn, H.; Dasgupta, S. Temperature-Dependent Performance of Printed Field-Effect Transistors with Solid Polymer Electrolyte Gating. *ACS applied materials & interfaces* **2016**, *8*, 31757–31763.

(25) Kinder, E. W.; Fuller, A.; Lin, Y. C.; Robinson, J. A.; Fullerton-Shirey, S. K. Increasing the Room-Temperature Electric Double Layer Retention Time in Two-Dimensional Crystal FETs. *ACS Applied Materials and Interfaces* **2017**, *9*, 25006–25013.

(26) Li, S.; Pei, F.; Ding, Y.; Guo, X.; Zhang, X.; Tao, H.; He, Z.; Hu, H.; Zhang, L. Metal-Organic Framework-Derived Elastic Solid Polymer Electrolytes Enabled by Covalent Crosslinking for High-Performance Lithium Metal Batteries. *Advanced Functional Materials* **2025**, *35*, 2415495.

(27) Liang, J.; Xu, K.; Arora, S.; Laaser, J. E.; Fullerton-Shirey, S. K. Ion-Locking in solid polymer electrolytes for reconfigurable gateless lateral graphene p-n junctions. *Materials* **2020**, *13*.

(28) Arora, S.; Liang, J.; Fullerton-Shirey, S. K.; Laaser, J. E. Triggerable Ion Release in Polymerized Ionic Liquids Containing Thermally Labile Diels-Alder Linkages. *ACS Materials Letters* **2020**, *2*, 331–335.

(29) Chen, Q. G.; Liao, W. T.; Li, R. Y.; Sanjuán, I.; Hsiao, N. C.; Ng, C. T.; Chang, T. T.; Guerrero, A.; Chueh, C. C.; Lee, W. Y. Organic Solid-State Electrolyte Synaptic Transistors with Photoinduced Thiol-Ene Cross-linked Polymer Electrolytes for Deep Neural Networks. *ACS Materials Letters* **2025**, *7*, 682–691.

(30) Winstein, S. et al. *1265 (1957), and accompanying papers*; 1959; Vol. 81; p 711.

(31) Kumar, S.; Qin, L.; Fan, L. S. *ACS Symposium Series*; American Chemical Society, 2020; Vol. 1364; pp 207–227.

(32) Dutta Dubey, K.; Stuyver, T.; Stuyver, T.; Kalita, S.; Shaik, S. Solvent Organization and Rate Regulation of a Menshutkin Reaction by Oriented External Electric Fields are Revealed by Combined MD and QM/MM Calculations. *Journal of the American Chemical Society* **2020**, *142*, 9955–9965.

(33) Shaik, S.; Ramanan, R.; Danovich, D.; Mandal, D. Structure and reactivity/selectivity control by oriented-external electric fields. *Chemical Society Reviews* **2018**, *47*, 5125–5145.

(34) Shaik, S.; Danovich, D.; Joy, J.; Wang, Z.; Stuyver, T. Electric-Field Mediated Chemistry: Uncovering and Exploiting the Potential of (Oriented) Electric Fields to Exert Chemical Catalysis and Reaction Control. 2020.

(35) Neumann, E. *Principles of electric field effects in chemical and biological systems*; Topics in Bioelectrochemistry and Bioenergetics, 1981; Vol. 4.

(36) Shaik, S.; Mandal, D.; Ramanan, R. Oriented electric fields as future smart reagents in chemistry. *Nature Chemistry* **2016**, *8*, 1091–1098.

(37) Cruickshank, J.; St A Hubbard, H. V.; Boden, N.; Ward, I. M. *The role of ionic salts in determining G and ionic conductivity in concentrated PEG electrolyte solutions*; 1995; Vol. 36; pp 3779–3781.

(38) Turan, H. T.; Brickel, S.; Meuwly, M. Solvent Effects on the Menshutkin Reaction. *Journal of Physical Chemistry B* **2022**, *126*, 1951–1961.

(39) Wei, D.; Shen, Y.; Huang, J.; Chen, Y.; Deng, Q.; Zhao, Y.; Ma, X. Fluorine ion contained polyionic liquid membranes with improved anion selectivity and CO2/N2 separation property. *Separation and Purification Technology* **2025**, *376*, 133853.

(40) Löwe, R.; Hanemann, T.; Hofmann, A. Polymerizable ionic liquids for solid-state polymer electrolytes. *Molecules* **2019**, *24*.

(41) Wu, H.; Cummings, O. T.; Wick, C. D. Computational investigation on the effect of alumina hydration on lithium ion mobility in poly(ethylene oxide) LiClO4 electrolytes. *The journal of physical chemistry. B* **2012**, *116*, 14922–14932.

(42) Giubileo, F.; Di Bartolomeo, A. The role of contact resistance in graphene field-effect devices. *Progress in Surface Science* **2017**, *92*, 143–175.

(43) Woeppel, A.; Xu, K.; Kozhakhmetov, A.; Awate, S.; Robinson, J. A.; Fullerton-Shirey, S. K. Single- versus Dual-Ion Conductors for Electric Double Layer Gating:

Finite Element Modeling and Hall-Effect Measurements. *ACS Applied Materials & Interfaces* **2020**, *12*, 40850–40858.

(44) Kim, S.; Lee, S. E.; Park, J. H.; Shin, J. Y.; Lee, B.; Lim, H. Y.; Oh, Y. T.; Hwang, J. P.; Seon, S. W.; Kim, S. H.; Yu, T. S.; Kim, B. H. High performance field-effect transistors based on partially suspended 2D materials via block copolymer lithography. *Polymers* **2021**, *13*, 1–10.

(45) Li, H. M.; Xu, K.; Bourdon, B.; Lu, H.; Lin, Y. C.; Robinson, J. A.; Seabaugh, A. C.; Fullerton-Shirey, S. K. Electric Double Layer Dynamics in Poly(ethylene oxide) LiClO4 on Graphene Transistors. *Journal of Physical Chemistry C* **2017**, *121*, 16996–17004.

(46) Xu, K.; Islam, M. M.; Guzman, D.; Seabaugh, A. C.; Strachan, A.; Fullerton-Shirey, S. K. Pulse Dynamics of Electric Double Layer Formation on All-Solid-State Graphene Field-Effect Transistors. *ACS Applied Materials & Interfaces* **2018**, *10*, 43166–43176.

(47) Liang, J.; Xu, K.; Toncini, B.; Bersch, B.; Jariwala, B.; Lin, Y. C.; Robinson, J.; Fullerton-Shirey, S. K. Impact of Post-Lithography Polymer Residue on the Electrical Characteristics of MoS 2 and WSe 2 Field Effect Transistors. *Advanced Materials Interfaces* **2019**, *6*.

(48) Shahalom, S.; Tong, T.; Emmett, S.; Saunders, B. R. Poly(DEAEMa-co-PEGMa): a new pH-responsive comb copolymer stabilizer for emulsions and dispersions. *Langmuir : the ACS journal of surfaces and colloids* **2006**, *22*, 8311–8317.

(49) Quiñonez-Angulo, P.; Ruiz-Villegas, J.; Licea-Claveríe, .; Ramirez-Jiménez, A.; Miranda-Soto, V.; Zapata-González, I. A kinetic study, thermal analysis and kinetic modeling on homo and copolymerization of 2-(N,N-diethylamino)ethyl methacrylate and PEGMA. *European Polymer Journal* **2018**, *109*, 347–359.

(50) Cheng, Z.; Zhu, X.; Shi, Z. L.; Neoh, K. G.; Kang, E. T. Polymer Microspheres with Permanent Antibacterial Surface from Surface-Initiated Atom Transfer Radical Polymerization. *Industrial and Engineering Chemistry Research* **2005**, *44*, 7098–7104.

(51) Ojima, K. O.; Dayarathne, S. H.; Kelly, M. T.; Zhao, B. Quaternary Ammonium-Containing Polyelectrolyte Brush Particles for Removal of Perrhenate Anion From Water: Effect of N-Substituents. *Macromolecular Rapid Communications* **2025**, *46*, 2401087.

Supplementary Files

This is a list of supplementary files associated with this preprint. Click to download.

- SupplementaryInformation.pdf
- SupplementaryInformation.zip